ACS APPLIED MATERIALS & INTERFACES

Research Article

www.acsami.org

# Origin of Effects of Additive Solvent on Film-Morphology in Solution-Processed Nonfullerene Solar Cells

Yuxia Chen, Xin Zhang, Chuanlang Zhan,* and Jiannian Yao

Beijing National Laboratory for Molecular Sciences, CAS Key Laboratory of Photochemistry, Institute of Chemistry, Chinese Academy of Sciences, Beijing 100190, People's Republic of China

Supporting Information

**ABSTRACT:** In this paper, we report an efficient nonfullerene solar cell based on small molecules of *p*-DTS(FBTTh$_2$)$_2$ and bis-PDI-T. Characterization data indicate that the nature of the acceptor aggregate is a key factor that affects the photocurrent. There is a good relationship between the short-circuit current density ($J_{SC}$) and the phase size of the acceptor-rich domains. The phase size of the acceptor-rich domains is tuned by both the additive types and additive content. As the kind of additive goes from 1-chloronaphthalene (CN) to 1,8-octanedithiol (ODT) and 1,8-diiodooctane (DIO), by this order the solubility of the acceptor in the additive is down, the phase size significantly decreases from over 400 nm down to 30 nm. Also, the acceptor's domain size decreases from 80 to 30 nm as the DIO content ([DIO]) is down from 1% to 0.15%. Following this trend, less DIO remains in the wet film as residue after the host chloroform evaporates, and thus less acceptor can be dissolved in the residue DIO. This decreasing of DIO content acts on the film-morphology similarly as the additive changes down to the one having a lower solubility. Accordingly, our results indicate that it is the dissolved amount of the organic component in the residue additive solvent of the wet film that plays a role in turning the phase size. The efficiency from this small molecule system is significantly raised from 0.02% up to 3.7% by selecting the additive type and fine-tuning the additive content.

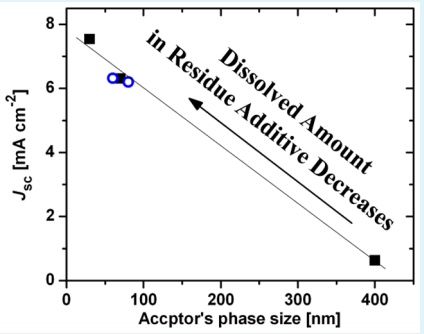


**KEYWORDS:** *nonfullerene acceptor, additive, solubility, exciton harvest, energy-transfer*

## 1. INTRODUCTION

In recent years, nonfullerene solar cells, which employ nonfullerene polymer/organic small molecule as the acceptor material, have been repaid increasing interest in the field of organic solar cells (OSCs).[1−12] The power conversion efficiency (PCE) of the state-of-the-art nonfullerene solar cell has been rapidly improved from below 4% to over 6%[13−16] in recent years, approaching the fullerene based counterparts. In the bulk-heterojunction (BHJ) OSCs, both the donor and acceptor are blended together at the nanoscale level, forming the light-harvesting active layer. To enhance the light-harvesting ability of the active layer of a nonfullerene solar cell, one of the current strategies is to complement the absorption spectrum of the blend nonfullerene acceptor with that of a low bandgap donor material, maximizing the usage of the solar photons.[1−4]

Nonfullerene acceptors, such as perylene diimide (PDI) based ones, show strong absorption in the visible wavelength region, typically <650 nm.[17,18] Exploitation of the excitons generated by the nonfullerene acceptor is as important as that of the donor's for the further improvement of the cell performance. Normally, the acceptor's excitons are exploited through the hole-transfer. By this path, the exciton randomly diffuses to the donor/acceptor (D/A) interface where the hole jumps to the donor molecule and the electron remains at the acceptor molecule, forming the so-called binding "electron−hole (*e-h*)" pair.[19] Organic semiconductors normally possess a low dielectric constant, and the exciton thus shows a large binding energy.[20] This large Coulombic attraction can, however, lead to significant recombination loss of the excitons during random diffusion. As a result the exciton diffusion length is normally short, typically about 10 nm.[21,22] To this end, engineering the acceptor aggregates in the blend film is the same important as the scientific selection of donor−acceptor system, for example, with complementary absorption spectra and matching frontier molecular orbitals.

Compared with the fullerene based counterpart, the efficient nonfullerene solar cell normally has a lower electron mobility than the hole mobility[13,14] and suffers stronger recombination loss, particularly, the geminate recombination.[23] This is likely due to the difference in the molecular structure between the fullerene and organic acceptors. The spherical shape of the fullerene molecule is helpful to form beneficial alignment with the donor molecules, affording efficient charge dissociation. From another aspect, it is easy for the fullerene acceptor to form interpenetrating nanoscale networks, which is available for the charge separation and transportation. However, both the organic donor and acceptor molecules are composed from

Received: October 31, 2014
Accepted: March 12, 2015
Published: March 12, 2015





DOI: 10.1021/am507581w
ACS Appl. Mater. Interfaces 2015, 7, 6462−6471

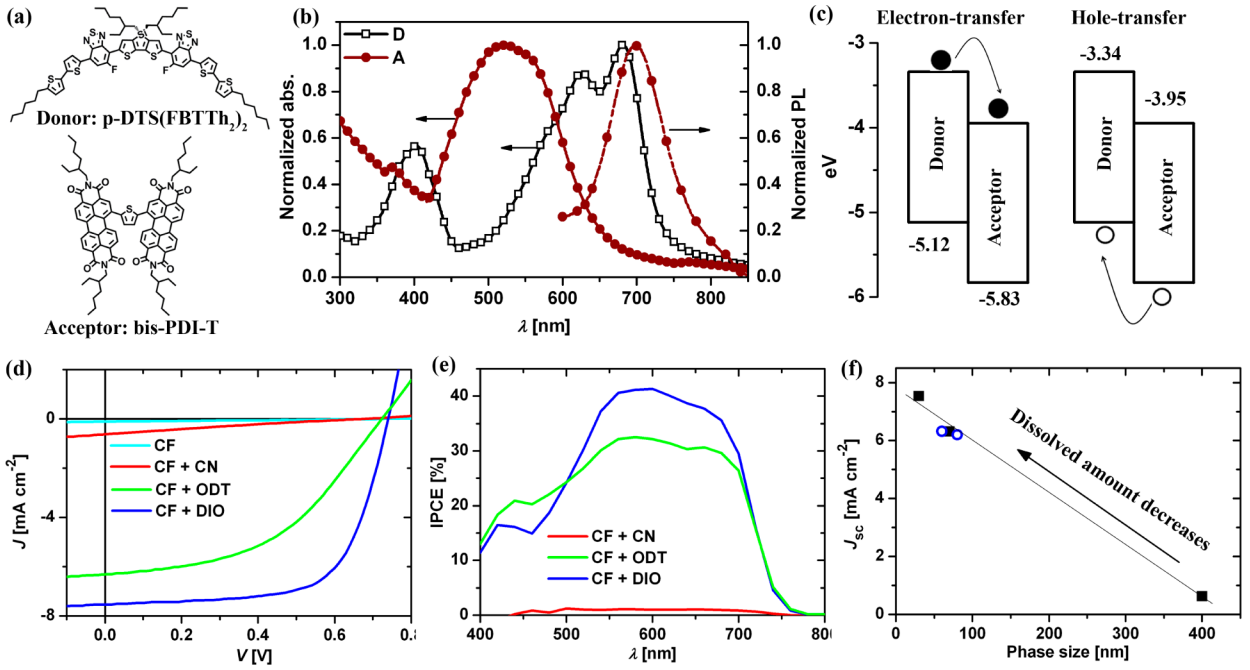


**Figure 1.** (a) Molecular structures of the donor and acceptor. (b) Normalized absorption (solid) and fluorescence (dash) spectra of the neat acceptor (circle) film and the absorption spectrum of the pure donor (square) film. The fluorescence spectrum is obtained upon excitation at 500 nm. (c) Diagram of the energy levels of donor and acceptor, and the electron- and hole-transfer, respectively, for the usage of the solar energy harvested by the donor and the acceptor phases. (d) Current density–voltage ($J$–$V$) curves and (e) IPCE spectra of the four best solar cells processing without or with additive. (f) Dependence of the $J_{SC}$s with the acceptor-rich dark phase sizes estimated from the TEM images of the relative solar cell blends. The dark squares represent the data from the CF+CN, CF+ODT, and CF+DIO, respectively, and the blue open circles are the data obtained from films with 0.5% and 1% DIO content ([DIO]), respectively.

planar organic $\pi$-moieties. Due to such similarity in molecular structure between the nonfullerene acceptor and organic donor, it is a big challenge to engineer the charge-separation and transportation favorable nanoscale film-morphology, which lags the realization of high-efficiency nonfullerene solar cells.

In this paper, our study clearly demonstrates that the film-morphology such as the phase size of the acceptor domains and the crystallinity of the donor phases in the solar cell blend can be efficiently tuned by controlling the dissolved amount of the organic components in the residue additive of the wet film. The dissolved amount is controlled by using different kinds of additives and different additive contents (v/v %). The afforded BHJ all small-molecule solar cell (All SMSC)[24−31] shows the best PCE of 3.7%.

## 2. RESULTS AND DISCUSSION

**2.1. Electric Performance of BHJ All SMSCs.** Figure 1a is the molecular structure of the selected small molecules, i.e., 7,7′(4,4-bis(2-ethylhexyl)-4H-silolo[3,2-b:4,5-b′]dithiophene-2,6-diyl)bis(6-fluoro-4-(5′-hexyl-[2,2′-bithiophen]-5-yl)benzo-[$c$][1,2,5]thiadiazole) (p-DTS(FBTTh$_2$)$_2$),[25] and 7,7′-(2,5-thienyl) bis-perylene diimide (bis-PDI-T).[26] The film absorption of this PDI acceptor is complementary to that of the donor (Figure 1b), enhancing the usage of the solar photons by the photoactive layer. Figure 1c gives the energy levels of the LUMO and the highest occupied molecular orbitals (HOMO) of the donor and acceptor. The D–A combination shows balanced energy offsets with $\Delta E_{LUMO} = E^{D}_{LUMO} - E^{A}_{LUMO} = 0.6$ eV and $\Delta E_{HOMO} = E^{D}_{HOMO} - E^{A}_{HOMO} = 0.7$ eV, which enables electron-transfer from the donor and efficient hole-transfer from the acceptor.

The use of additive is a well-known method to improve the performance of both the fullerene and nonfullerene solar cells.[14,27,28] According to published studies, as an additive has a higher-boiling point ($T_b$) than the host solvent or/and it can selectively dissolve one component of the donor and acceptor, the use of additive may provide sufficient time for the blend components to self-organize and to phase segregation, which enhances the device performance.[29,30] Herein, we select 1-chloronaphthalene (CN), 1,8-octanedithiol (ODT), and 1,8-diiodooctane (DIO) as additives. As Table 1 shows, CN and ODT have close boiling points ($T_b$) and slightly different solubility differences between the donor and the acceptor, i.e., solubility ratios, ($S_D/S_A$). In contrast, ODT and DIO have different $T_b$, but identical solubility ratios. The All SMSC solar cell devices are fabricated with this D–A combination as the photoactive layer, and use chloroform (CF) as the host solvent and each of CN, ODT, and DIO as the additive. Table S1 in

**Table 1. Boiling Point of the Selected Solvent, And the Solubility of the Donor and Acceptor in the Host and Additive Solvents**

| solvent | $T_b$ [°C] | $S_D$ [b] [mg/mL] | $S_A$ [b] [mg/mL] | $S_D/S_A$ [c] |
|---|---|---|---|---|
| CF | 61 | 2 | 3 | 0.7 |
| CN | 259 | 21 | 6 | 3.5 |
| ODT | 269 | 0.2 | 0.04 | 5 |
| DIO | 333 | 0.1 | 0.02 | 5 |

[a]The solubilities (in mg/mL) are all tested at room temperature. [b]$S_D$ and $S_A$ represent the absolute solubility of the donor and the acceptor in the neat solvent. [c]$S_D/S_A$ represents the solubility ratio of the donor and the acceptor in the same solvent.



DOI: 10.1021/am507581w
ACS Appl. Mater. Interfaces 2015, 7, 6462−6471

**Table 2. Photovoltaic and Morphological Parameters of the Films Processed without or with Additives, And with Different DIO Contents**

| Solvent | cell parameters (av.[a]) | | | | phase size | |
|---|---|---|---|---|---|---|
| | PCE [%] | $J_{SC}$ [mA·cm$^{-2}$] | $V_{OC}$ [V] | FF [%] | bright [nm] | dark [nm] |
| CF | 0.02 (0.02 ± 0.00) | 0.11 (0.09 ± 0.01) | 0.75 (0.78 ± 0.02) | 27.3 (27.4 ± 0.47) | 5 | 5 |
| CF+CN | 0.09 (0.09 ± 0.02) | 0.63 (0.68 ± 0.07) | 0.68 (0.61 ± 0.06) | 22.2 (23.9 ± 1.3) | 40 | >400 |
| CF+ODT | 2.13 (1.95 ± 0.09) | 6.31 (6.28 ± 0.10) | 0.72 (0.70 ± 0.01) | 47.0 (44.7 ± 1.8) | 40 | 70 |
| CF+DIO (0.15%) | 3.70 (3.47 ± 0.13) | 7.54 (7.31 ± 0.23) | 0.74 (0.73 ± 0.00) | 66.1 (65.3 ± 2.2) | 40 | 30 |
| CF+DIO (0.5%) | 2.09 (2.04 ± 0.04) | 6.32 (6.22 ± 0.09) | 0.67 (0.66 ± 0.00) | 49.4 (48.6 ± 0.6) | 40 | 60 |
| CF+DIO (1%) | 1.57 (1.54 ± 0.04) | 6.20 (6.04 ± 0.16) | 0.62 (0.62 ± 0.01) | 40.9 (41.5 ± 0.6) | 40 | 80 |

[a]Average values from 10 devices and standard deviations are given in the braces.

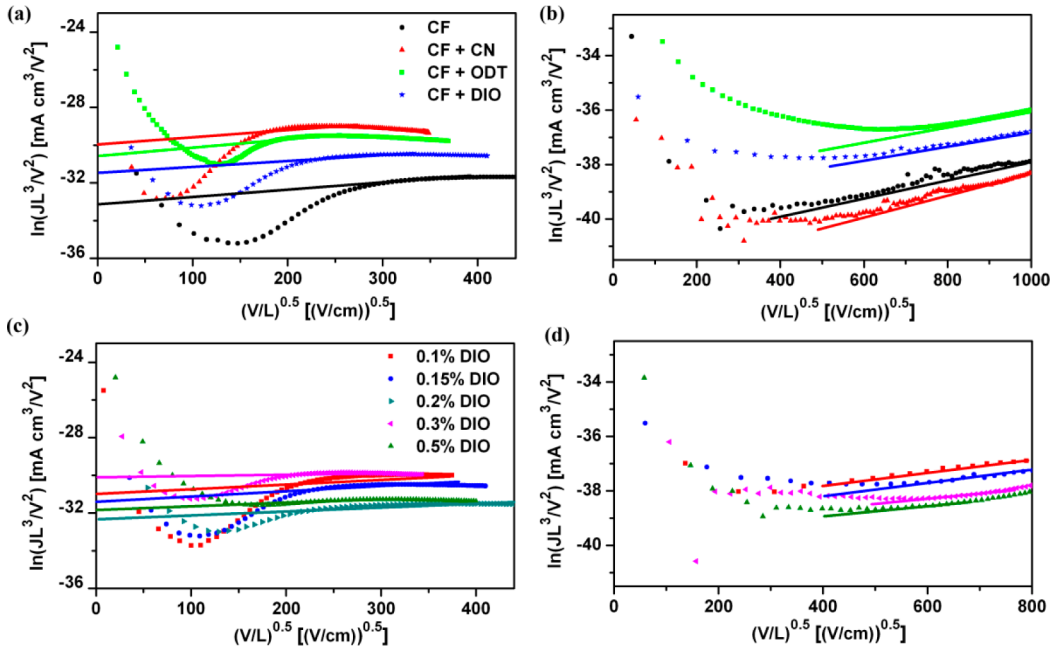


**Figure 2.** Plots of $\ln(JL^3/V^2)$ vs $(V/L)^{0.5}$ extracted from the solar cell blends fabricated without additive and with different additives (a and b) or with different [DIO]s (c and d) on the basis of the hole-only (a and c) and electron-only devices (b and d).

the Supporting Information shows the parameters of the solar cells optimized under different content of each additive. The best PCE appears at an intermediate content of additive, which is a common phenomenon for the use of additive in the field of BHJ OCSs.

Table 2 collects the photovoltaic data of the best solar cells optimized under different conditions. We name the solar cells and their relative blends prepared without additive (i.e., pure CF) and with 0.3% CN, 0.4% ODT, and 0.15% DIO as CF's, CF+CN's, CF+ODT's, and CF+DIO's, respectively. Figure 1d is the current density ($J$)−voltage ($V$) curves from the related best cells. The CF's solar cell shows much inferior performance with a PCE < 0.02%. After using additive, the best value of the short-circuit current density ($J_{SC}$) increases from 0.63 (CF +CN) to 6.31 (CF+ODT), and then 7.54 mA/cm$^2$ (CF+DIO), and the fill factor (FF) increases from 22.2 to 47.0 and then 66.1%. Following this order, the best PCE significantly increases from 0.09 to 2.13 and 3.70%. The incident photon-to-electron conversion efficiency (IPCE) (Figure 1e and Table S2 in the Supporting Information) enhances in accordance with the increase of the $J_{SC}$. If we turn back to Table 1, we can see that the $J_{SC}$, FF, and PCE all increase with the decrease of the absolute solubility value of the donor ($S_D$) and the acceptor ($S_A$) in the pure additive $S_D$ and $S_A$.

Both the hole and electron mobilities are estimated by the space-charge-limited current (SCLC) method. The electron-only and hole-only devices are ITO/TIPD/donor:acceptor/Al and ITO/PEDOT:PSS/donor:acceptor/Au, respectively. The electron and hole mobilities were extracted by fitting the current density−voltage curves using the following equation $\ln(JL^3V^2) = 0.89(1/E_0)^{0.5}(V/L)^{0.5} + \ln(9\varepsilon\varepsilon_0\mu/8)$.[31,32] Figure 2 gives the plots of $\ln(JL^3/V^2)$ vs $(V/L)^{0.5}$ and Table S1 in the Supporting Information collects the estimated mobility data from the intercept value of $\ln(9\varepsilon\varepsilon_0\mu_0/8)$. One can see that (1) the hole mobility increases by 1 order of magnitude after use of additive and (2) hole mobility is always higher than the electron mobility under each condition, suggesting that the lower electron mobility is a factor limiting the scale of the photocurrent.

**2.2. Evolution of Crystallinity.** The donor is highly crystalline and its crystallinity can be controlled by the additive content, as reported previously.[28] Change of crystallinity of the solar cell blends are studied by two-dimensional grazing-incidence X-ray diffraction (2D-GIXRD) (Figures S1 and S2 in the Supporting Information). Figure 3 gives the linecut profiles along the out-of-plane and in-plane direction from the 2D-GIXRD images of the pure donor and acceptor films, and the solar cell blends obtained using different kinds of additives


DOI: 10.1021/am507581w
ACS Appl. Mater. Interfaces 2015, 7, 6462−6471

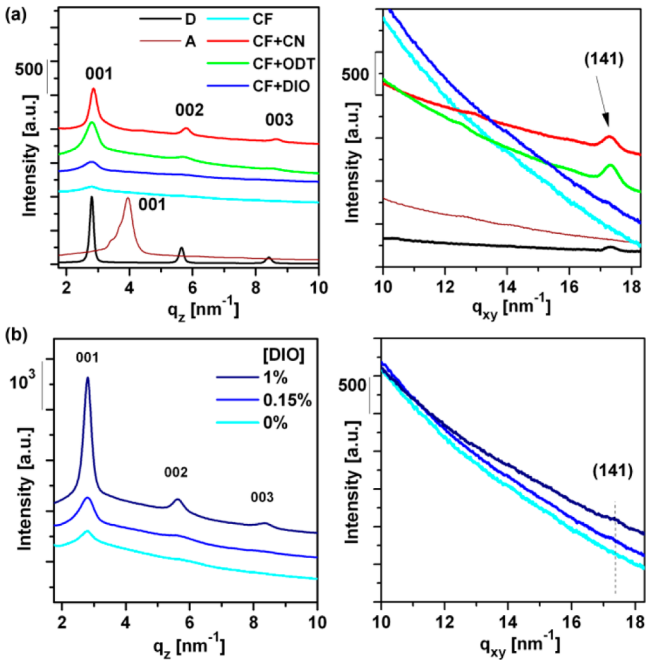


**Figure 3.** Linecut profiles along the out-of-plane and in-plane direction, both from the 2D-GIXRD images (Figures S1 and S2 in the Supporting Information) of the neat donor and acceptor film, the blends (a) from CF, CF+DIO, CF+CN, and CF+ODT and (b) with 0, 0.15, and 1% DIO, respectively.

(Figure 3a) and under three [DIO]s of 0%, 0.15% and 1% (Figure 3b), respectively. With respect to the highly crystallinity of the donor, the acceptor is amorphous and no relative signals are observed from the blends. The (100), (200), and (300) as well as the (141)[28] diffractions from the donor are clearly observed and their intensity all becomes weaker and the band becomes broader as the used additive goes from CN to ODT and DIO. The variation in the width of the (100) peak is related to the change of correlation lengths of the donor crystallites, which can be estimated by the Scherrer Equation $L = K\lambda/\beta \cos\theta$,[33] where $L$ is the correlation lengths, $K$ is Scherrer constants, $\beta$ is the full width at half-maximum of the diffraction peak in radians, $\lambda$ is the incident wavelength, and $\theta$ is the diffraction angle. Table S3 in the Supporting Information shows the calculated values of the correlation length. The correlation length becomes shorter with the additive going from CN to ODT and DIO, by this order the solubility of the donor decreases.

The host solvent of chloroform evaporates completely after spin-coating and the high-boiling point additive remains in the wet film as residue. Lower value of the solubility shown in Table 1 as the additive goes from CN to ODT and then DIO indicates less organic component dissolving in the residue additive in the wet film. Similarly, a decrease of the [DIO] indicates less DIO remains in the wet film as the residue and less donor (acceptor) is dissolved in the residue DIO. As a result, a decrease of the [DIO] acts on the crystallinity similarly to the change of the additive from one with a high solubility to another with a low solubility. Figure 3b illustrates that all the diffractions from the donor becomes weaker and the band becomes broader upon the decrease of the [DIO], indicating a shorter correlation length of the crystallites (Table S3 in the Supporting Information).

Figure 4 displays the absorption spectra of the neat donor film and solar cell blend films obtained under different

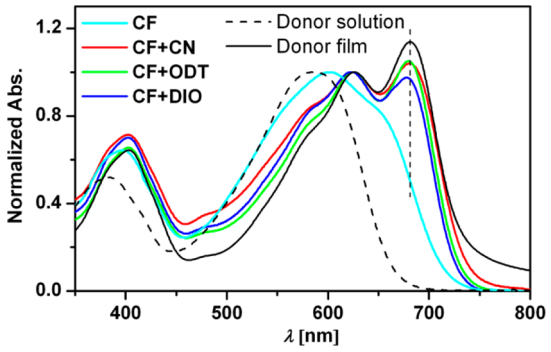


**Figure 4.** Absorption spectra of the donor solution with a concentration of $10^{-6}$ M in CF and neat donor film and the solar cell blends casting without or with additive of 0.3% CN, 0.4% ODT, and 0.15% DIO, respectively.

conditions. As the donor is transitioned from the dilute CF solution to pristine crystalline film, the absorption band is significantly red-shifted with two peaks appearing at 620 and 680 nm, respectively, suggesting the formation of the crystalline donor film. With respect to the featureless absorption band of the CF's blend, emergence of the 620 and 680 nm peaks demonstrates the formation of crystalline donor domains after the use of additive. The intensity of the 680 nm peak becomes weaker and the long-wavelength edge is slightly blue-shifted as the used additive goes from CN to ODT and DIO. The absorption spectrum changes following the same trend as the [DIO] decreases from 0.5% to 0.1% (Figure S3 in the Supporting Information). Taken together, the absorption spectra demonstrate that the crystallinity of the donor phases becomes smaller either as the additive goes from CN to ODT and DIO or as the [DIO] decreases, which is in line with that trend from the 2D-GIXRD data. With respect to the crystalline nature of the donor phases, the acceptor phases are relatively amorphous, which is in line with the data of the carrier mobilities, i.e., the electron mobility is always lower than the hole mobility.

**2.3. Evolution of Phase Size.** The use of additive is generally followed with a change in the film-morphology. Figure 5 shows the typical transmission electron microscopy (TEM) images of the solar cell blends under different conditions. The CF's solar cell blend shows negligible phase segregation, whereas the blends after using additive all give contrasted white and dark domains. In these TEM images with a D/A weight ratio of 3:1, the bright phases are more frequently observed. When the D/A weight ratio decreases to 1:3, the dark phases are observed more frequently (Figure S4 in the Supporting Information). This suggests that the dark phases are the acceptor-rich domains, whereas the bright ones are the donor-rich phases. We should point out that such assignments need other evidence to further confirm. The phase size of the acceptor-rich dark domains reduces from 400 to 70 and 30 nm as the used additive goes from CN to ODT and then DIO (Figure 5b–d), following this order the solubility of the acceptor in the additive decreases (Table 1). Similarly, the dark domains changes from fiber-like to particle-like and the phase size decreases from 80 to 60 and 30 nm when the [DIO] decreases from 1% to 0.5% and 0.15%. In a striking contrast, the size of the white fibrils is kept constant at 40 nm either after


DOI: 10.1021/am507581w
ACS Appl. Mater. Interfaces 2015, 7, 6462–6471

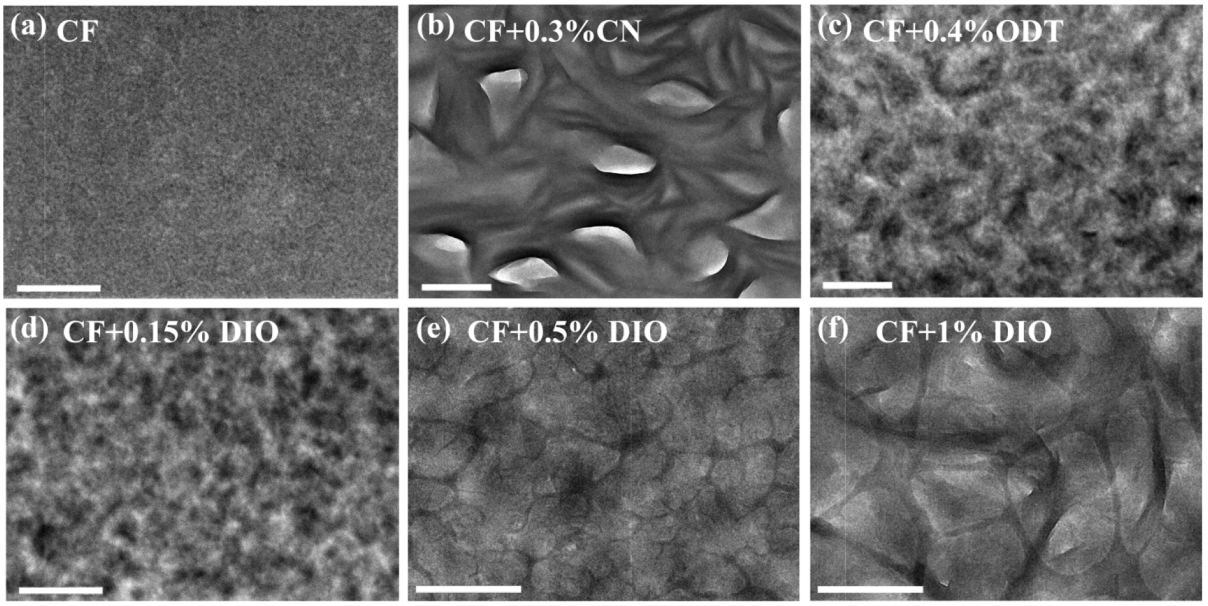


**Figure 5.** TEM image of the blend films (with a D/A weight ratio of 3:1) prepared from pure CF (a) and with 0.3% CN (b), 0.4% ODT (c), 0.15% DIO (d), 0.5% DIO (e), and 1% DIO (f), respectively. The scale bars are 400 nm.

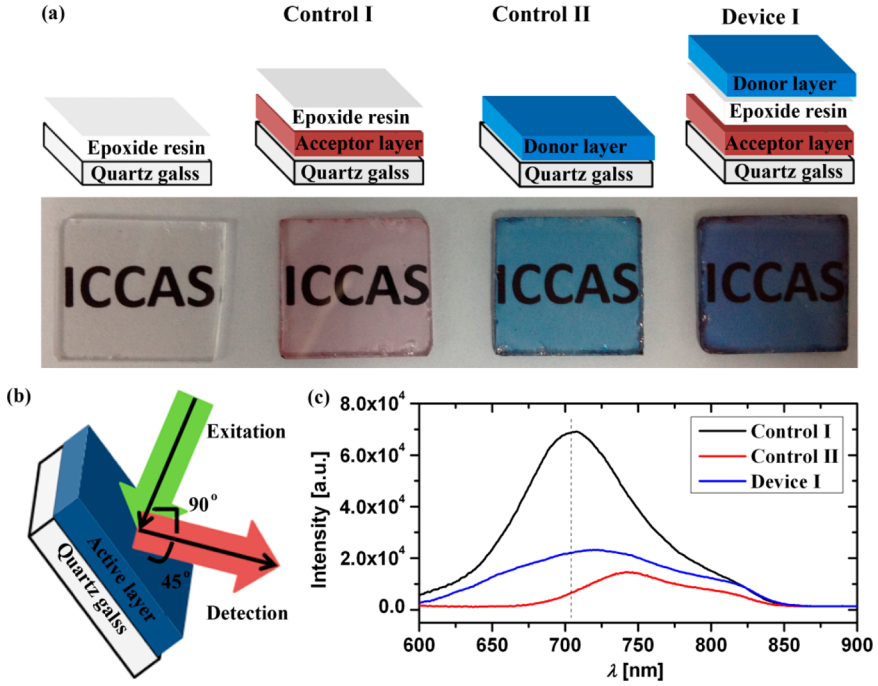


**Figure 6.** (a) Structures of the planar devices of Device I and Control I and II and their photos showing semitransparent nature of the planar devices. (b) Depiction of the experiments regarding the excitation and fluorescence collection for Device I and Control I and II. (c) Fluorescence spectra of Device I and Control I and II. All fluorescence spectra are obtained under excitation at 530 nm and with the same instrument parameters.

the use of ODT and DIO as the additive or after the use of different [DIO]'s (Figure 5c–f). The white fibers tend to aggregate at a higher DIO content, forming cluster-like domains. Atomic force microscopy (AFM) height and phase images (Figures S5 and S6 in the Supporting Information) also reveal a decrease of the phase size and the roughness-mean-square (rms) either when the additive changes from CN to ODT and ODT or when the DIO content decreases.

As mentioned in sections 2.1 and 2.2, both the data of the carrier mobility and the crystallinity suggest that the amorphous nature of the acceptor phases is likely a factor limiting the scale of the photocurrent. In this part of section 2.3, the TEM data indicates that the phase size of the acceptor-rich dark domains is obviously affected by the additive kind and content, while the size of the donor-rich white fibers is little varied. As Figure 1f displays, there is a good relationship between the $J_{SC}$ value and the dark phase size. Such a phenomenon is in agreement with the reported observation from the dependence of the EQE value with the phase size, in which the phase size of the polymer donor decreases with the decrease of the solubility of the blend polymer donor in the host solvent and the maximum EQE value increases linearly as a result.[34] We kindly note that


DOI: 10.1021/am507581w
ACS Appl. Mater. Interfaces 2015, 7, 6462–6471

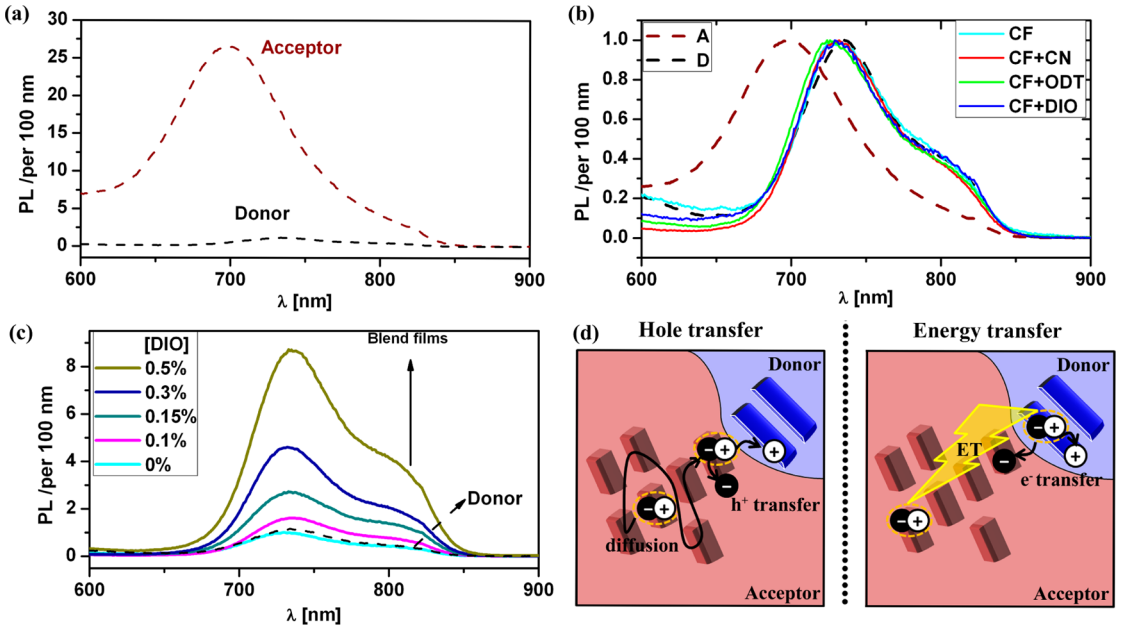


**Figure 7.** (a) Fluorescence spectra of pristine donor and acceptor film (dash), and their blend films (solid) (b) with different kinds of additives and (c) with the increased DIO contents. All fluorescence spectra are obtained under excitation at 530 nm and with the same instrument parameters. (d) Schematic image of hole-transfer and energy-transfer pathways for the exciton harvesting in acceptor phase.

when the adding DIO content is less than 0.15%, the $J_{SC}$ does not follow the linear plot with the phase size. This is probably because in these cases (including the one without additive) the $J_{SC}$ is affected not only by the acceptor phase size but also by the phase segregation.

**2.4. Possible Energy-Transfer from Nonfullerene Acceptor to Donor in the BHJ Blend Film.** As Figure 1b shows, the fluorescence spectrum from the pure acceptor film overlaps with the absorption spectrum of the pure donor, which enables energy-transfer from the acceptor to the donor. There are already some studies on the energy-transfer from supernumerary component to the host donor/acceptor.[35−39] However, energy-transfer between the host donor and nonfullerene acceptor is still little known to us. To confirm the energy-transfer from the acceptor to the donor in solid film, we fabricated a double layer device with a structure of quartz glass/acceptor (25 nm)/epoxide resin (10 nm)/donor (20 nm) (Device I, Figure 6a), in which the intermediate layer of epoxide resin was used to avoid possible electron and hole-transfer between the acceptor and donor layers. Two control device of quartz glass/acceptor (25 nm)/epoxide resin (10 nm) and quartz glass/donor (20 nm) (Control I and II, Figure 6a) were fabricated for comparisons. The acceptor and donor layers of the Control I and II were prepared under the same condition with Device I, and the film thickness of the acceptor layer in Control I and that of the donor layer in Control II are both identical to that of the corresponding layer in Device I. Figure 6b depicts the experiments regarding the excitation and fluorescence collection. Figure 6c gives the fluorescence spectra and detected intensity from these three planar devices. For all the three devices, the fluorescence is excited using the 530 nm light and collected from the top surface of the organic layer, i.e., from the epoxide resin surface for Control I and the top surface of the donor layer for Control II and Device I. The epoxide resin layer is transparent with a transmittance of 98.7% (Figure S7 of the Supporting Information) at 530 nm. The thicknesses of the epoxide layer in Control I and Device I are identical to each other (both 10 nm). The effect of the parasitic absorption from the epoxide layer on the fluorescence of Device I over the Control I can be ruled out. One can see from Figure 6c that the fluorescence from the acceptor in Device I is significantly quenched with respect to that from Control I ($I_{fl}$, 6.9 vs 2.2 × $10^4$ a.u.). One may wonder that the donor layer atop the epoxide/acceptor one in Device I should absorb the 530 nm light with respect to Control I, which should contributes to the fluorescence decrease. We kindly point out that the excitation light power for the fluorescence measurement is usually much higher than the fluorescence intensity of the experimental sample, for example, our cases. We can thus rule out the effect of the light absorption from the top donor layer on the fluorescence intensity of the epoxide capped acceptor layer. Accordingly, the fluorescence decrease from the acceptor layer in Device I over that from Control I indicates the presence of energy-transfer from the acceptor layer to the donor.

Upon excitation at 530 nm, the fluorescence intensity from the pure acceptor film is stronger than that of the donor by 26-fold (26.6 vs 1.1 a.u. per 100 nm of the film thickness) (Figure 7a). When the acceptor is blended with the donor together, forming BHJ structure, the band shape (Figure 7b) and intensity (Figure 7c) of the fluorescence from the CF's blend are both identical to those from the pure donor film. The fluorescence from each of the CF+DIO's, CF+ODT's, and CF +CN's blends features very much like that from the pure donor film, too (Figure 7b). These two facts from the fluorescence spectra clearly indicate that the fluorescence from the acceptor is totally quenched in the BHJ solar cell blends. More interestingly, the fluorescence intensity from the blend film increases continuously with the [DIO] (Figure 7c).

Because the energy-transfer does exist in the blend, going from the nonfullerene acceptor to the blend donor, it should act as complementary pathways with the hole-transfer for the solar cell to harvest the acceptor excitons (Figure 7d), contributing to the complete quenching of the acceptor fluorescence and the increasing donor fluorescence. The


DOI: 10.1021/am507581w
ACS Appl. Mater. Interfaces 2015, 7, 6462−6471

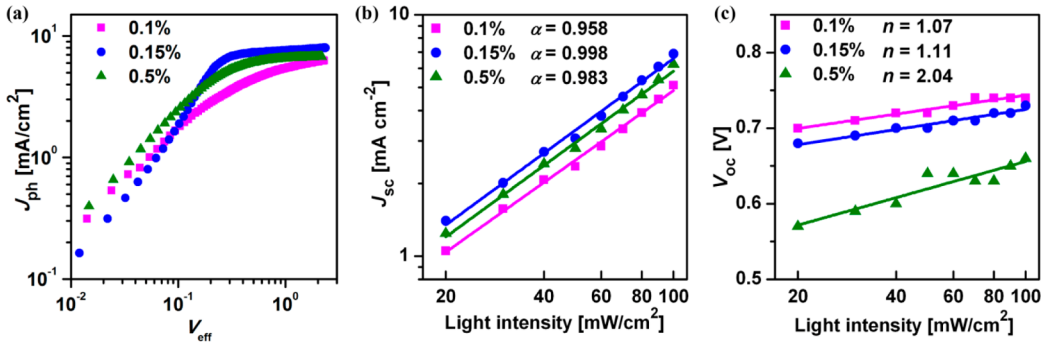


**Figure 8.** (a) Plots of $J_{ph}$ vs $V_{eff}$, and light intensity dependence of the $J_{SC}$ (b) and $V_{OC}$ (c) for the devices with 0.1, 0.15, and 0.5% DIO, respectively. The $\alpha$ and $n$ are determined from the linear fitting (solid lines) to the experimental data.

donor excitons are exploited through the electron-transfer. Although the phase size of the donor-rich fibers are kept constant at ca. 40 nm, the formation of the cluster domains of the donor-rich fibers should have negative effect on the charge-transfer. In other words, the aggregation of the donor-rich fibers upon the increase of the [DIO] is unfavorable to the electron-transfer. The decrease of the electron-transfer and the existence of the energy-transfer from the nonfullerene acceptor both act on the increase of the fluorescence of the solar cell blends.

Except for the charge-transfer appearing between the blend donor and acceptor, other kinds of nonradiative pathways may act on the fluorescence emission, especially for the highly crystalline donor aggregates. The fluorescence quantum yield of the donor is 22.71 and 1.32 in chloroform solution and in neat film, respectively, indicating the fluorescence of the donor is strongly quenched (by 17.2-fold) after transitioning from the solution (molecular) to film (aggregate) state. The fluorescence quantum yield of the acceptor is 4.01 and 2.52 in chloroform solution and in neat film, respectively, indicating that the aggregation-induced fluorescence quenching is very weak for the acceptor (only by 1.59-fold). This is well consistent with the highly crystalline nature of the donor and the amorphous characteristics of the acceptor. As the data of the 2D-GIXRD (Figure 3b) and absorption spectra (Figure S3 in the Supporting Information), the crystallinity of the donor phases in the solar cell blend gradually becomes greater and greater with the increase of the [DIO]. The improvement of the crystallinity of the donor phases should accompany with an enhancement of the fluorescence quenching, due to the strong aggregation-induced fluorescence quenching effect of the donor. Therefore, the contribution from the nonradiative recombinations other than the electron-transfer should become greater and the fluorescence should be quenched more at a higher [DIO]. However, the experimental intensity of the fluorescence from the blend films is enhanced continuously, following the increase of the [DIO] (Figure 7c). This suggests that the fluorescence enhancement upon the increase of the [DIO] might be excluded from the contribution from nonradiative pathways (with the electron-transfer excluded). Otherwise, the aggregation-induced fluorescence quenching effect is weak for the acceptor. We can reasonably assume that the acceptor domains in the BHJ solar cell blend should photofluoresce, as the neat acceptor film does. Its intensity should become stronger with the increase of the [DIO] because the hole-transfer becomes weaker with the increase of the phase size. However, the experimental fact demonstrates that no fluorescence is detected from the blend acceptor. Taken together, the analyses on the aggregation-induced fluorescence quenching of both the donor and acceptor again suggest that the energy-transfer contributes to the fluorescence increase of the blend films, accompanying with the increase of the [DIO], as shown in Figure 7c.

Taken together, the above data demonstrates that the electron-, hole-, and energy-transfer are all related to the increase of the fluorescence of the solar cell blends. Unfortunately, the data in hands cannot allow us to quantitatively determine the contributions from the three pathways, i.e., energy-, hole-, and electron-transfer, to the fluorescence emission of the blend films. This is particularly due to the complexity of the distribution of the donor and acceptor phases, the formation of the nanoscale interpenetrating networks in the BHJ blend film and the unclear structure of the donor−acceptor interfaces.

**2.5. Carrier Generation, Collection and Recombination Loss.** The photocurrent is scaled by the photogenerated carrier concentration, which is related to several factors such as the maximum *e-h* pair generation rate ($G_{max}$) of solar cell, collection, and recombination loss. To see the effects of the phase size on the recombination of the mobile carriers for this small molecule system, we hereafter select three DIO contents as examples because the above results clearly indicate that the decrease of the DIO content acts on the phase size in a similar way with the change of the additive type from CN to ODT and DIO. Figure 8a plots the photocurrent ($J_{ph}$) vs effective applied voltage ($V_{eff}$) at three [DIO]s, in which $J_{ph} = J_L - J_D$, where $J_L$ and $J_D$ are the current measured under illumination ($J_L$) and in the dark ($J_D$), respectively, and $V_{eff} = V_0 - V_{app}$, $V_{app}$ is the applied voltage, $V_0$ is the compensation voltage, which is defined as the voltage when $J_{ph} = 0$ mA/cm$^2$. At the low $V_{eff}$ range, where $V_{app}$ is close to $V_0$, implying a small electric field in the device, $J_{ph}$, the photocurrent increases linearly with the effective voltage, whereas at the high $V_{eff}$ range, $J_{ph}$ enters the saturation regime, where almost all the photogenerated bound *e-h* pairs are dissociated, forming free charge carriers, and are drifted to the right electrode.[40] As a result, the saturated photocurrent ($J_{ph,sat}$) can be expressed by $G_{max}$ with $J_{ph,sat} = eLG_{max}$, where $e$ is the electric charge and $L$ is the thickness of the active layer.[40−42] As shown in Figure 8a, the $J_{ph,sat}$ increases from 0.1% (6.24 mA cm$^{-2}$) to 0.15% DIO (7.98 mA cm$^{-2}$), but decreases at 0.5% DIO (6.72 mA cm$^{-2}$). The calculated $G_{max}$ changes from 4.6 to 5.6 and to 5.0 × 10$^{27}$ m$^{-3}$ s$^{-1}$, which increases first and then turn down as the [DIO] is over 0.15%.

The monomolecular/bimolecular recombination losses were studied by the incident light power dependent $J-V$ characteristics. At short-circuit where the $V_{eff}$ is large, the photogenerated


DOI: 10.1021/am507581w
ACS Appl. Mater. Interfaces 2015, 7, 6462−6471

electrons and holes are efficiently swept out of the device prior to recombination. This recombination is described using $J_{SC} \propto P^{\alpha}$ (Figure 8b). The fitting value of $\alpha$ is 0.958, 0.998, and 0.983, respectively, as the DIO content is 0.1, 0.15, and 0.5%. All values are close to unity, indicating the monomolecular dominates the recombination loss at short-circuit.[43,44] At open-circuit where all of the photogenerated free carriers recombine, recombination mechanism can be reflected by the formula: $V_{OC} \propto nkT/q\ln(P)$ (Figure 8c), where $k$, $T$, and $q$ are the Boltzmann constant, temperature in Kelvin, and the elementary charge, respectively.[45] The value of fitting $n$ is 1.07, 1.11, and 2.04, respectively. The $V_{OC}$ exhibits stronger light power dependence in the device as the [DIO] is 0.5% than 0.1 and 0.15%. The $n$ value deviating from unity means that the monomolecular recombination is involved and a larger $n$ value indicates more serious loss.[43−45] Accordingly, the recombination data suggests that a higher [DIO] than 0.15% leads to more serious loss of the free carriers. This may be related with the formation of clusters of the donor-rich fibers and larger acceptor-rich dark domains, both of which are yielded by a higher [DIO] (Figure 5). The slight decrease of the $J_{SC}$ is consistent with the larger $n$ value as the [DIO] is over 0.15%.

It should be noted that as the [DIO] is over 0.15%, the $J_{SC}$ only slightly decreases with the value down from 7.54 to 6.20 mA/cm$^2$ (Table 2) even as the [DIO] reaches 1%. This is strikingly different from that observed from the $PC_{71}BM$ based cells with the same molecule as the donor and using similar device structures, in which the device performance is progressively increased and followed by a rapid deterioration as the DIO content is over 0.4%.[25] The slight decrease of the $J_{SC}$ at [DIO] > 0.15% could be an evidence for the participation of the energy-transfer, which complements the decrease of hole-transfer to exploit the acceptor excitons at a higher DIO content level, as the acceptor's phase size becomes larger.

Evidence also comes from the comparisons of the EQE spectrum of the solar cell and the absorption spectrum of the corresponding blend (Figure S3 in the Supporting Information), both are obtained at a [DIO] of 0.1, 0.15, and 0.5%, respectively. It can be seen that in the absorption spectra of the three blends, the absorption around 520 nm are always much weaker than those around 650 nm ($A_{520\ nm}$:$A_{650\ nm} \approx 0.4$), whereas the EQE response at the absorption wavelength region of the acceptor (around 520 nm) are comparable with those at absorption region of donor (around 650 nm) ($EQE_{520\ nm}$:$EQE_{650\ nm} \approx 0.8$). It can be seen that the EQE response ratio is 2 times the absorption ratio of the acceptor and donor. This again demonstrates that the energy-transfer may contribute to the EQE response, and, further the photocurrent. However, it is hardly to quantity the contribution from energy-transfer. In fact, the obtained maximum photocurrent in device with an intermediate content of DIO is a result of fine-turned phase-segregation and phase size, which compromise the electron-, hole-, and energy-transfer, and also the charge transportation.

## 3. CONCLUSIONS

An efficient all small-molecule BHJ solar cell with a PCE of 3.7% is obtained from a unique nonfullerene small molecule system of $p$-DTS(FBTTh$_2$)$_2$ and bis-PDI-T. The phase size of the donor-rich fiber is kept constant, whereas that of the acceptor-rich domains is reduced by reducing the dissolved amount of the organic component in the residue additive in the wet film after spin-coating. The reduction of the dissolved amount of the organic component is achieved by either changing the used additive from one having a high solubility to another one with a lower solubility of the component, or by decreasing the additive content (by which the residue additive in the wet film becomes less and the dissolved amount of component thus becomes less). It is clear that the amorphous acceptor-rich domains play a key role in scaling the photocurrent and there is a good relationship between the $J_{SC}$ and the phase size of the acceptor-rich domains.

## 4. EXPERIMENTAL SECTION

**Device Construction and Measurement.** Indium tin oxide (ITO) coated substrates were precleaned and treated with UV−$O_3$ to further remove the organic residues. Then they were coated with PEDOT:PSS (poly(3,4-ethylenedioxythiophene):poly(styrenesulfonate)) (ca. 30 nm) and annealed in oven at 150 °C for 15 min. After that, active layers of p-DTS(FBTTh$_2$)$_2$:bis-PDI-T were spin-coated on the substrate from a $CHCl_3$ solution at a total concentration of 12 mg mL$^{-1}$. Finally, Ca (ca. 20 nm) and Al (ca. 80 nm) were thermally evaporated on top of the organic layer to make the sandwiched structure ITO/PEDOT:PSS/active layers/Ca/Al. The active area of the device was 0.06 cm$^2$ and the thickness of the photoactive layers was about 100 nm. The current−voltage measurements were carried out in the dark as well as under simulated 100 mW cm$^{-2}$ AM1.5G light source, using a computer-controlled Keithley 2400 Source Measure Unit. The EQE measurements of devices were performed in air with oriel IQE 200 (Newport) with a scanning rate of 20 nm per datum point.

## ■ ASSOCIATED CONTENT

### Ⓢ Supporting Information

Experimental details, device fabrication, and complete characterization of devices. This material is available free of charge via the Internet at http://pubs.acs.org.

## ■ AUTHOR INFORMATION

### Corresponding Author

*Prof. Chuanlang Zhan, Professor of Chemistry. Phone: 0086-10-82617312. E-mail: clzhan@iccas.ac.cn.

### Notes

The authors declare no competing financial interest.

## ■ ACKNOWLEDGMENTS

This work was financially supported by NSFC (No. 91433202, 21327805, 91227112, and 21221002), Chinese Academy of Sciences (XDB12010200), and MOST (Project 973, 2011CB808400 and 2012YQ120060). Beijing Synchrotron Radiation Facility (BSRF) is acknowledged for the GIXRD measurements.

## ■ REFERENCES

(1) Zhou, Y.; Kurosawa, T.; Ma, W.; Guo, Y.; Fang, L.; Vandewal, K.; Diao, Y.; Wang, C.; Yan, Q.; Reinspach, J.; Mei, J.; Appleton, A. L.; Koleilat, G. I.; Gao, Y.; Mannsfeld, S. C. B.; Salleo, A.; Ade, H.; Zhao, D.; Bao, Z. High Performance All-Polymer Solar Cell via Polymer Side-Chain Engineering. *Adv. Mater.* **2014**, *26*, 3767−3772.

(2) Lu, Z.; Jiang, B.; Zhang, X.; Tang, A.; Chen, L.; Zhan, C.; Yao, J. Perylene−Diimide Based Non-fullerene Solar Cells with 4.34% Efficiency through Engineering Surface Donor/Acceptor Compositions. *Chem. Mater.* **2014**, *26*, 2907−2914.

(3) Zhou, N.; Lin, H.; Lou, S. J.; Yu, X.; Guo, P.; Manley, E. F.; Loser, S.; Hartnett, P.; Huang, H.; Wasielewski, M. R.; Chen, L. X.; Chang, R. P. H.; Facchetti, A.; Marks, T. J. Morphology-Performance Relationships in High-Efficiency All-Polymer Solar Cells. *Adv. Energy Mater.* **2014**, *4*, 1300785.



DOI: 10.1021/am507581w
*ACS Appl. Mater. Interfaces* 2015, 7, 6462−6471

(4) Zang, Y.; Li, C. Z.; Chueh, C. C.; Williams, S. T.; Jiang, W.; Wang, Z. H.; Yu, J. S.; Jen, A. K. Integrated Molecular, Interfacial, and Device Engineering towards High-Performance Non-fullerene based Organic Solar Cells. *Adv. Mater.* **2014**, *26*, 5708−5714.
(5) Mori, D.; Benten, H.; Okada, I.; Ohkita, H.; Ito, S. Highly Efficient Charge-Carrier Generation and Collection in Polymer/Polymer Blend Solar Cells with a Power Conversion Efficiency of 5.7%. *Energy Environ. Sci.* **2014**, *7*, 2939−2943.
(6) Cheng, P.; Ye, L.; Zhao, X. G.; Hou, J. H.; Li, Y. F.; Zhan, X. W. Binary Additives Synergistically Boost the Efficiency of All-Polymer Solar Cells up to 3.45%. *Energy Environ. Sci.* **2014**, *7*, 1351−1356.
(7) Eftaiha, A. a. F.; Sun, J.-P.; Hill, I. G.; Welch, G. C. Recent Advances of Non-fullerene, Small Molecular Acceptors for Solution Processed Bulk Heterojunction Solar Cells. *J. Mater. Chem. A* **2014**, *2*, 1201−1213.
(8) Jung, I.; Lo, W.; Jang, J.; Chen, W.; Zhao, D.; Landry, E.; Lu, L.; Talapin, D.; Yu, L. Synthesis and Search for Design Principles of New Electron Accepting Polymers for All-Polymer Solar Cells. *Chem. Mater.* **2014**, *26*, 3450−3459.
(9) Zheng, Y. Q.; Dai, Y. Z.; Zhou, Y.; Wang, J. Y.; Pei, J. Rational Molecular Engineering towards Efficient Non-fullerene Small Molecule Acceptors for Inverted Bulk Heterojunction Organic Solar Cells. *Chem. Commun.* **2014**, *50*, 1591−1594.
(10) Yan, Q. F.; Zhou, Y.; Zheng, Y. Q.; Pei, J.; Zhao, D. H. Towards Rational Design of Organic Electron Acceptors for Photovoltaics: A Study Based on Perylenediimide Derivatives. *Chem. Sci.* **2013**, *4*, 4389−4394.
(11) Zhou, Y.; Ding, L.; Shi, K.; Dai, Y. Z.; Ai, N.; Wang, J.; Pei, J. A Non-fullerene Small Molecule as Efficient Electron Acceptor in Organic Bulk Heterojunction Solar Cells. *Adv. Mater.* **2012**, *24*, 957−961.
(12) Ye, T.; Singh, R.; Butt, H. J.; Floudas, G.; Keivanidis, P. E. Effect of Local and Global Structural Order on the Performance of Perylene Diimide Excimeric Solar Cells. *ACS Appl. Mater. Interfaces* **2013**, *5*, 11844−11857.
(13) Zhao, J.; Li, Y.; Lin, H.; Liu, Y.; Jiang, K.; Mu, C.; Ma, T.; Lin Lai, J. Y.; Hu, H.; Yu, D.; Yan, H. High-Efficiency Non-fullerene Organic Solar Cells Enabled by a Difluorobenzothiadiazole-based Donor Polymer Combined with a Properly Matched Small Molecule Acceptor. *Energy Environ. Sci.* **2015**, *8*, 520−525.
(14) Zhang, X.; Zhan, C.; Yao, J. Non-fullerene Organic Solar Cells with 6.1% Efficiency through Fine-Tuning Parameters of the Film-Forming Process. *Chem. Mater.* **2015**, *27*, 166−173.
(15) Lin, Y.; Zhang, Z.-G.; Bai, H.; Wang, J.; Yao, Y.; Li, Y.; Zhu, D.; Zhan, X. High-Performance Fullerene-Free Polymer Solar Cells with 6.31% Efficiency. *Energy Environ. Sci.* **2015**, *8*, 610−616.
(16) Zhong, Y.; Trinh, M. T.; Chen, R.; Wang, W.; Khlyabich, P. P.; Kumar, B.; Xu, Q.; Nam, C. Y.; Sfeir, M. Y.; Black, C.; Steigerwald, M. L.; Loo, Y. L.; Xiao, S.; Ng, F.; Zhu, X. Y.; Nuckolls, C. Efficient Organic Solar Cells with Helical Perylene Diimide Electron Acceptors. *J. Am. Chem. Soc.* **2014**, *136*, 15215−21.
(17) Shivanna, R.; Shoaee, S.; Dimitrov, S.; Kandappa, S. K.; Rajaram, S.; Durrant, J. R.; Narayan, K. S. Charge Generation and Transport in Efficient Organic Bulk Heterojunction Solar Cells with a Perylene Acceptor. *Energy Environ. Sci.* **2014**, *7*, 435−441.
(18) Jiang, W.; Ye, L.; Li, X.; Xiao, C.; Tan, F.; Zhao, W.; Hou, J.; Wang, Z. Bay-Linked Perylene Bisimides as Promising Non-fullerene Acceptors for Organic Solar Cells. *Chem. Commun.* **2014**, *50*, 1024−1026.
(19) Gelinas, S.; Rao, A.; Kumar, A.; Smith, S. L.; Chin, A. W.; Clark, J.; van der Poll, T. S.; Bazan, G. C.; Friend, R. H. Ultrafast Long-Range Charge Separation in Organic Semiconductor Photovoltaic Diodes. *Science* **2014**, *343*, 512−516.
(20) Holcombe, T. W.; Norton, J. E.; Rivnay, J.; Woo, C. H.; Goris, L.; Piliego, C.; Griffini, G.; Sellinger, A.; Bredas, J. L.; Salleo, A.; Frechet, J. M. Steric Control of the Donor/Acceptor Interface: Implications in Organic Photovoltaic Charge Generation. *J. Am. Chem. Soc.* **2011**, *133*, 12106−12114.
(21) Peumans, P.; Yakimov, A.; Forrest, S. R. Small Molecular Weight Organic Thin-Film Photodetectors and Solar Cells. *J. Appl. Phys.* **2003**, *93*, 3693−3723.
(22) Scully, S. R.; McGehee, M. D. Effects of Optical Interference and Energy Transfer on Exciton Diffusion Length Measurements in Organic Semiconductors. *J. Appl. Phys.* **2006**, *100*, 034907−1.
(23) Sharenko, A.; Gehrig, D.; Laquai, F.; Nguyen, T.-Q. The Effect of Solvent Additive on the Charge Generation and Photovoltaic Performance of a Solution-Processed Small Molecule:Perylene Diimide Bulk Heterojunction Solar Cell. *Chem. Mater.* **2014**, *26*, 4109−4118.
(24) Huang, J.; Wang, X.; Zhang, X.; Niu, Z.; Lu, Z.; Jiang, B.; Sun, Y.; Zhan, C.; Yao, J. Additive-Assisted Control over Phase-Separated Nanostructures by Manipulating Alkylthienyl Position at Donor Backbone for Solution-Processed, Non-fullerene, All-Small-Molecule Solar Cells. *ACS Appl. Mater. Interfaces* **2014**, *6*, 3853−3862.
(25) van der Poll, T. S.; Love, J. A.; Nguyen, T.-Q.; Bazan, G. C. Non-basic High-Performance Molecules for Solution-Processed Organic Solar Cells. *Adv. Mater.* **2012**, *24*, 3646−3649.
(26) Lu, Z.; Zhang, X.; Zhan, C.; Jiang, B.; Zhang, X.; Chen, L.; Yao, J. Impact of Molecular Solvophobicity vs. Solvophilicity on Device Performances of Dimeric Perylene Diimide based Solution-Processed Non-fullerene Organic Solar Cells. *Phys. Chem. Chem. Phys.* **2013**, *15*, 11375−11385.
(27) Peet, J.; Kim, J. Y.; Coates, N. E.; Ma, W. L.; Moses, D.; Heeger, A. J.; Bazan, G. C. Efficiency Enhancement in Low-Bandgap Polymer Solar Cells by Processing with Alkane Dithiols. *Nat. Mater.* **2007**, *6*, 497−500.
(28) Perez, L. A.; Chou, K. W.; Love, J. A.; van der Poll, T. S.; Smilgies, D.-M.; Nguyen, T.-Q.; Kramer, E. J.; Amassian, A.; Bazan, G. C. Solvent Additive Effects on Small Molecule Crystallization in Bulk Heterojunction Solar Cells Probed During Spin Casting. *Adv. Mater.* **2013**, *25*, 6380−6384.
(29) Lee, J. K.; Ma, W. L.; Brabec, C. J.; Yuen, J.; Moon, J. S.; Kim, J. Y.; Lee, K.; Bazan, G. C.; Heeger, A. J. Processing Additives for Improved Efficiency from Bulk Heterojunction Solar Cells. *J. Am. Chem. Soc.* **2008**, *130*, 3619−3623.
(30) Lou, S. J.; Szarko, J. M.; Xu, T.; Yu, L.; Marks, T. J.; Chen, L. X. Effects of Additives on the Morphology of Solution Phase Aggregates Formed by Active Layer Components of High-Efficiency Organic Solar Cells. *J. Am. Chem. Soc.* **2011**, *133*, 20661−20663.
(31) Tan, Z.; Zhang, W.; Zhang, Z.; Qian, D.; Huang, Y.; Hou, J.; Li, Y. High-Performance Inverted Polymer Solar Cells with Solution-Processed Titanium Chelate as Electron-Collecting Layer on ITO Electrode. *Adv. Mater.* **2012**, *24*, 1476−1481.
(32) An, Z. S.; Yu, J. S.; Jones, S. C.; Barlow, S.; Yoo, S.; Domercq, B.; Prins, P.; Siebbeles, L. D. A.; Kippelen, B.; Marder, S. R. High Electron Mobility in Room-Temperature Discotic Liquid-Crystalline Perylene Diimides. *Adv. Mater.* **2005**, *17*, 2580−2583.
(33) Langford, J. I.; Wilson, A. J. C. Scherrer after Sixty Years: A Survey and Some New Results in the Determination of Crystallite Size. *J. Appl. Crystallogr.* **1978**, *11*, 102−113.
(34) Li, W. W.; Hendriks, K. H.; Furlan, A.; Roelofs, W. S. C.; Wienk, M. M.; Janssen, R. A. J. Universal Correlation between Fibril Width and Quantum Efficiency in Diketopyrrolopyrrole-based Polymer Solar Cells. *J. Am. Chem. Soc.* **2013**, *135*, 18942−18948.
(35) Cnops, K.; Rand, B. P.; Cheyns, D.; Verreet, B.; Empl, M. A.; Heremans, P. 8.4% Efficient Fullerene-Free Organic Solar Cells Exploiting Long-Range Exciton Energy Transfer. *Nat. Commun.* **2014**, *5*, 3406−3411.
(36) Griffith, O. L.; Forrest, S. R. Exciton Management in Organic Photovoltaic Multidonor Energy Cascades. *Nano Lett.* **2014**, *14*, 2353−2358.
(37) Lu, L.; Xu, T.; Chen, W.; Landry, E. S.; Yu, L. Ternary Blend Polymer Solar Cells with Enhanced Power Conversion Efficiency. *Nat. Photonics* **2014**, *8*, 716−722.
(38) Huang, J.-S.; Goh, T.; Li, X.; Sfeir, M. Y.; Bielinski, E. A.; Tomasulo, S.; Lee, M. L.; Hazari, N.; Taylor, A. D. Polymer Bulk


DOI: 10.1021/am507581w
*ACS Appl. Mater. Interfaces* 2015, 7, 6462−6471

Heterojunction Solar Cells Employing Förster Resonance Energy Transfer. *Nat. Photonics* **2013**, *7*, 479−485.
(39) Chen, D. Y.; Chen, C. L.; Cheng, Y. M.; Lai, C. H.; Yu, J. Y.; Chen, B. S.; Hsieh, C. C.; Chen, H. C.; Chen, L. Y.; Wei, C. Y.; Wu, C. C.; Chou, P. T. Design and Synthesis of Trithiophene-Bound Excited-State Intramolecular Proton Transfer Dye: Enhancement on the Performance of Bulk Heterojunction Solar Cells. *ACS Appl. Mater. Interfaces* **2010**, *2*, 1621−1629.
(40) Mihailetchi, V. D.; Koster, L. J.; Hummelen, J. C.; Blom, P. W. Photocurrent Generation in Polymer-Fullerene Bulk Heterojunctions. *Phys. Rev. Lett.* **2004**, *93*, 216601.
(41) Goodman, A. M.; Rose, A. Double Extraction of Uniformly Generated Electron-Hole Pairs from Insulators with Noninjecting Contacts. *J. Appl. Phys.* **1971**, *42*, 2823−2830.
(42) Kyaw, A. K. K.; Wang, D. H.; Wynands, D.; Zhang, J.; Nguyen, T. Q.; Bazan, G. C.; Heeger, A. J. Improved Light Harvesting and Improved Efficiency by Insertion of an Optical Spacer (ZnO) in Solution-Processed Small-Molecule Solar Cells. *Nano Lett.* **2013**, *13*, 3796−3801.
(43) Koster, L. J.; Kemerink, M.; Wienk, M. M.; Maturova, K.; Janssen, R. A. Quantifying Bimolecular Recombination Losses in Organic Bulk Heterojunction Solar Cells. *Adv. Mater.* **2011**, *23*, 1670−1674.
(44) Schilinsky, P.; Waldauf, C.; Brabec, C. J. Recombination and Loss Analysis in Polythiophene based Bulk Heterojunction Photodetectors. *Appl. Phys. Lett.* **2002**, *81*, 3885−3887.
(45) Shuttle, C. G.; O'Regan, B.; Ballantyne, A. M.; Nelson, J.; Bradley, D. D. C.; Durrant, J. R. Bimolecular Recombination Losses in Polythiophene: Fullerene Solar Cells. *Phys. Rev. B* **2008**, *78*, 113201.


DOI: 10.1021/am507581w
*ACS Appl. Mater. Interfaces* 2015, 7, 6462−6471